Y/DW-1352

Y-12

OAK RIDGE Y-12 PLANT

MARTIN MARIETTA

NONDESTRUCTIVE TESTING OF CERAMIC COMPONENTS

COOPERATIVE RESEARCH AND DEVELOPMENT AGREEMENT COMPLETION REPORT

D. A. Carpenter, T. W. Dews,
M. W. Moyer, R. E. Oakes

Instrumentation & Characterization Department
Development Division

December 22, 1994

Prepared by the
Oak Ridge Y-12 Plant
managed by
MARTIN MARIETTA ENERGY SYSTEMS, INC.
for the
U.S. DEPARTMENT OF ENERGY
under contract DE-AC05-84OR21400

MANAGED BY
MARTIN MARIETTA ENERGY SYSTEMS, INC.
FOR THE UNITED STATES
DEPARTMENT OF ENERGY
UCN-13672 (2 10-90)

Y/DW-1352

NONDESTRUCTIVE TESTING OF CERAMIC COMPONENTS

COOPERATIVE RESEARCH AND DEVELOPMENT AGREEMENT COMPLETION REPORT

CRADA Number: Y-1291-0051

D. A. Carpenter, T. W. Dews,
M. W. Moyer, R. E. Oakes

Instrumentation & Characterization Department Development Division

December 22, 1994

Prepared by the
Oak Ridge Y-12 Plant
managed by
MARTIN MARIETTA ENERGY SYSTEMS, INC.
for the
U.S. DEPARTMENT OF ENERGY
under contract DE-AC05-84OR21400

TJ

TABLE OF CONTENTS

LIST OF FIGURES

LIST OF TABLES

ABSTRACT

In a joint Cooperative Research and Development Agreement (CRADA) between Martin Marietta Energy Systems (MMES) and an industrial partner, Y-12 has been evaluating nondestructive evaluation (NDE) techniques to identify the quality of high strength aluminum oxide tubes used in laser applications. In Phase I, several NDE techniques were developed to inspect the tubes. In Phase II a correlation between detected defects, actual failure mode and strength of the tubes was developed. In Phase II the industrial partner supplied tubes manufactured under a variety of conditions and containing material defects expected from process control variations. The tubes were inspected at MMES utilizing a variety of available acoustic techniques. After inspection, ring tensile specimens were fabricated to determine the tensile strength. The data were evaluated utilizing Weibull statistics to determine the statistical impact of the defects upon strength and correlate the data with the nondestructive evaluations of the tubes and observed defect distribution.

INTRODUCTION

A Cooperative Research and Development Agreement (CRADA) was set up between Martin Marietta Energy Systems and an industrial partner to evaluate the fabrication of ceramic tubes. Increasingly stringent requirements on the quality and consistency of ceramic tubes used in laser applications has convinced the industrial partner that standard testing techniques are not adequate. These tubes have been found to have cracks and defects on or near the inside wall which cause the tubes to fail prematurely during service. The CRADA was set up to evaluate several nondestructive evaluation (NDE) techniques for determining material properties and detecting detrimental conditions (both defects and material property variations) in order to better understand the correlation between material properties, defects, and strength of the tubes. NDE inspection techniques including ultrasonics, ultrasonic spectroscopy (RUS), radiography, surface analysis techniques, and thermal techniques have the potential of identifying detrimental conditions. These techniques were evaluated and the most promising techniques evaluated on a set of tubes fabricated specifically to test the tube strength. The results of the NDE test development and the evaluation of tube strength using a ring tensile test are described in this report.

PHASE I EFFORT

The industrial partner has supplied several samples fabricated under a variety of conditions and containing a variety of defects including pits and cracks. In addition, several aluminum oxide three-point bend specimens were obtained as part of another program. A listing and description of the available samples are given in Table I. The Phase I effort centered around identifying NDE techniques which would be able to detect defects and variations in material condition. Several NDE techniques were evaluated on these specimens and the results are given below.

Thermal Inspection

Several aluminum oxide disk samples were inspected using a thermal imaging system to determine whether thermal imaging would be an effective method for identifying surface flaws in aluminum oxide laser tubes manufactured by the industrial partner.

A Model 600 Infrared Imaging Radiometer was used for scanning 2 inch diameter aluminum oxide disks containing surface defects. Thermal images of the samples under test were displayed in color with corresponding palette related to temperature. The ceramic samples were mounted in a sheet of carbon-bonded carbon fiber (CBCF). CBCF was selected for mounting the samples because of its property of being an excellent thermal absorber. The disks were first illuminated from the back with a heat source while the thermal images were monitored in real-time from the opposite side. The CBCF shielded the imaging system so the samples could be viewed without interference from stray radiation emitted by the heater. In a second set of experiments the samples were illuminated with the heat source, turned toward the radiometer, and monitored while they returned to equilibrium.

Though there were notable increases (or decreases) in the digital temperature readout over the surface of the disk under test, there were no detectable changes in the displayed image. Defects on samples that had visually obvious surface flaws could not be correlated with any features in the images under any of the experimental conditions. It appears that the thermal diffusivity of the aluminum oxide samples is too high to allow the system to detect the defects in the samples.

The results obtained from the testing of these material samples indicate that the use of thermal imaging to monitor the surface of alumina laser tubes during a heating or cooling cycle is not a viable method of identifying surface defects.

X-Radiography

Tubes F1, F2, and F3 were radiographed to determine the sensitivity of radiography to internal and near surface defects. In tube F1, radiography was able to detect an ID wall pit. The location of this pit was marked on the OD surface with a graphite pencil. Cracks in tubes were not detected on radiographs. The problem with radiography is that it is not sensitive to tight cracks and several radiographs must be taken to get full coverage of the tube.

Ultrasonic Inspection

Two types of ultrasonic inspection were set up to inspect the ceramic tubes supplied by the industrial partner. A through transmission inspection was used to detect loss of signal. A transmitting transducer mounted on a search tube with a right angled mirror were inserted into the tube. A receiving transducer on the outside of the tube detected the signal. Water was used as a couplant. Figure 1 shows the setup of the inspection. This inspection is sensitive to any defect that reduces the signal transmitted through the wall of the tube. In addition,

Table I - Available Aluminum Oxide Samples for Phase I Study

Sample ID	Sample Description	Sample Conditions	Inspection Techniques Tried	Techniques That Detected Conditions
998-5	3 point bend specimen for velocity measurements, 99.8% density	small grains (5-10 μm)	UT(PE), AV	AV
998-8	3 point bend specimen for velocity measurements, 99.8% density	dual phase (5-10 μm & 30-50 μm) grains	UT(PE), AV	AV
998-10	3 point bend specimen for velocity measurements, 99.8% density	small grains (5-10 μm)	UT(PE), AV	AV
940-14	3 point bend specimen for velocity measurements, 94% density	15-25 μm grains 10-15 μm porosity	UT(PE), AV	AV, UT(PE)
L1	~11.7" x 2.2" x 0.33" thick	none	UT(TT), AV	
L2	~0.8" x 1.1" x 0.25" thick	none	UT(TT), AV	
L3	~2.0" x 0.9" x 0.38" thick	none	UT(TT), AV	
L4	2.4" dia x 0.35" thick	none	UT(TT), AV	
L5	~1.0" x 0.9" x 0.43" thick	none	UT(TT), AV	
S4	1.5" dia x 0.78" thick	none	UT(TT), AV, Th	
S5	1.55" dia x 0.73" thick	none	UT(TT), AV, Th	
G1	Tube 6" long	Rough OD surface	UT(SW,TT), RT	UT(SW,TT)
G2	Tube 6" long	none	UT(SW,TT), RT	
G3	Tube 6" long	none	UT(SW,TT), RT	
F1	Tube 6" long	ID pit	UT(SW,TT), RT	UT(SW), RT
F2	Tube 6" long	Short ID Crack	UT(SW,TT), RT	UT(SW)
F3	Tube 6" long	ID Surface wound	UT(SW,TT), RT	UT(SW)
LT1	Tube 7.65" long - part 1 of 23" tube	none	UT(SW,TT)	
LT2	Tube 7.55" long - part 2 of 23" tube	ID Pits internal defect	UT(SW,TT) UT(SW,TT)	UT(SW,TT) UT(TT)
LT3	Tube 7.7" long - part 3 of 23" tube	none	UT(SW,TT)	
C1	Tube 2.35" long	crack	UT(SW,TT)	UT(SW,TT)
C2	Tube 1.4" long	crack	UT(SW,TT)	UT(SW,TT)
T1	Tube 2.65" long - lower density	crack	UT(SW,TT),	UT(SW,TT),
C3E	Tube 3.0" long with big end	cracks	UT(SW,TT)	UT(SW,TT)
C4E	Tube 4.7" long with big end	cracks	UT(SW,TT)	UT(SW,TT)

Inspection Techniques:
UT Ultrasonic Testing
SW - Surface Wave
PE - Pulse Echo Inspection
TT - Through Transmission Inspection
AV Acoustic Velocity Measurements
RT Radiographic Inspection
Th Thermal Inspection
XRM X-ray Microprobe Inspection

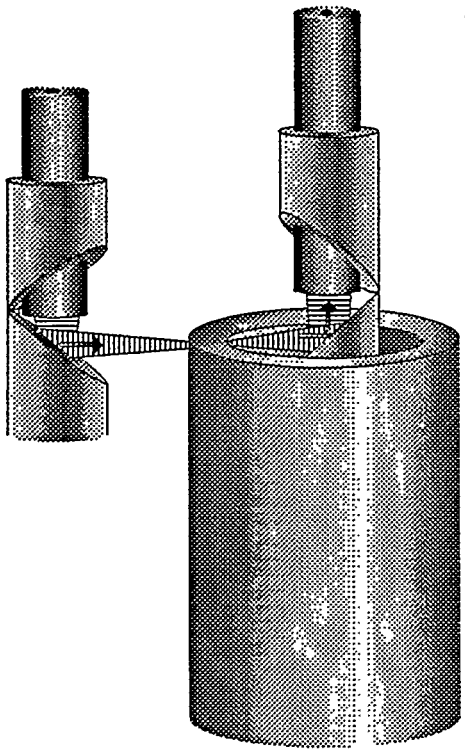

Figure 1. Setup for Through Transmission Scans of Aluminum Oxide Tubes

a radial surface wave inspection was developed which is sensitive to near surface anomalies regardless of the orientation of the defect. The technique relies on the use of a short focus transducer that produces radial surface waves from the periphery of the transducer. The surface waves constructively interfere with the longitudinal wave from the center of the transducer. This interference signal is sensitive to small variations in material properties and to defects within approximately one wavelength of the surface. A 15 MHz transducer was used which produces a surface wave penetration of approximately 0.015 inches. The setup is shown in Figure 2. The surface wave inspection was able to detect the surface breaking cracks in the tubes. The scan was also sensitive to small surface scratches. Figure 3 is a composite figure that shows the surface wave inspection of the OD surface of tube F1 with zoomed insets of the OD and ID surface wave scans of the area containing an ID surface pit. The scan of the OD surface shows the presence of surface scratches which were left when the tube was sanded with emery paper while in the green state before firing. During radiography, the location of the ID pit was marked with a graphite pencil on the tube OD. This graphite circle is easily detected by the surface wave inspection on the tube OD. The ID surface wave scan shows the image of the pit on the tube ID surface. The resolution of the flaw is much better using the ultrasonic technique than using the radiographic technique.

Through transmission scans appear to be more reliable in detecting tight cracks than the surface wave inspection. Cracks will tend to produce a larger target through the thickness of the part wall and can thus be detected with a lower resolution scan. The same crack will produce a much narrower indication in the radial surface wave scan than it produces in the through transmission scan. Figure 4 shows a through transmission scan of tube T1 which contains a through the wall crack with inset scans of the OD and ID radial surface wave inspections. Near the top of the tube, the crack was oriented perpendicular to the tube wall. The crack rotated as it propagated down the tube. The through transmission scan shows a narrow indication with only a slight reduction in signal where the crack is perpendicular to the tube wall. With this crack orientation, the ultrasonic beam propagates on both sides of the crack. As the crack orientation rotates, the crack obscures a larger portion of the beam causing a larger loss of signal. The radial surface wave inspection images the crack as it breaks the tube wall surface. Note that the ID wall scan images the top edge of the crack which breaks the ID surface while the OD wall scan images the bottom edge of the crack which breaks the OD surface. The through transmission scan is also sensitive to internal flaws. Figure 5 shows the through transmission image of a portion of tube LT2 which contains an OD scratch, an ID surface flaw and an internal flaw. The figure contains inset zoom images of all three defects. At the bottom of the figure, the insets show that the through transmission scan detects both the OD scratch and the ID flaw. The OD surface wave scan detects the OD scratch while the ID surface wave scan detects the ID flaw. At the right of the figure, the insets show that the through transmission scan detects the internal flaw but neither of the surface wave scans can detect the flaw.

X-Ray Microprobe Inspection

Tube T1 which had a crack (ultrasonic scan shown in Figure 3) was also inspected using x-ray microprobe (XRM). The XRM excites x-ray fluorescence in the elements of the specimen using a microbeam of x-rays. In the scanning mode, element homogeneity can be determined and inclusions can be detected and identified. Zirconium and iron were detected in x-ray microfluorescence (XRMF) images of specimen T1. Figure 6 shows relatively large zirconium-containing particles (green) in a crack in specimen T1, while smaller zirconium and iron (red) particles were distributed more uniformly throughout the matrix. The matrix (blue) was imaged using Compton scatter radiation, which is strongly scattered by aluminum oxide. It is possible that the two zirconium-containing particles shown in Figure 6 could act as crack-initiation sites.

Acoustic Property Measurements

By measuring the longitudinal and shear velocities and the density of a sample, other sample velocities (extensional and Rayleigh velocities) and material properties (Young's modulus, shear modulus, bulk modulus and Poisson's Ratio) may be calculated. Velocity measurements were made on three high density and one low density three point bend specimens. One of the high density specimens had a dual population of grains.

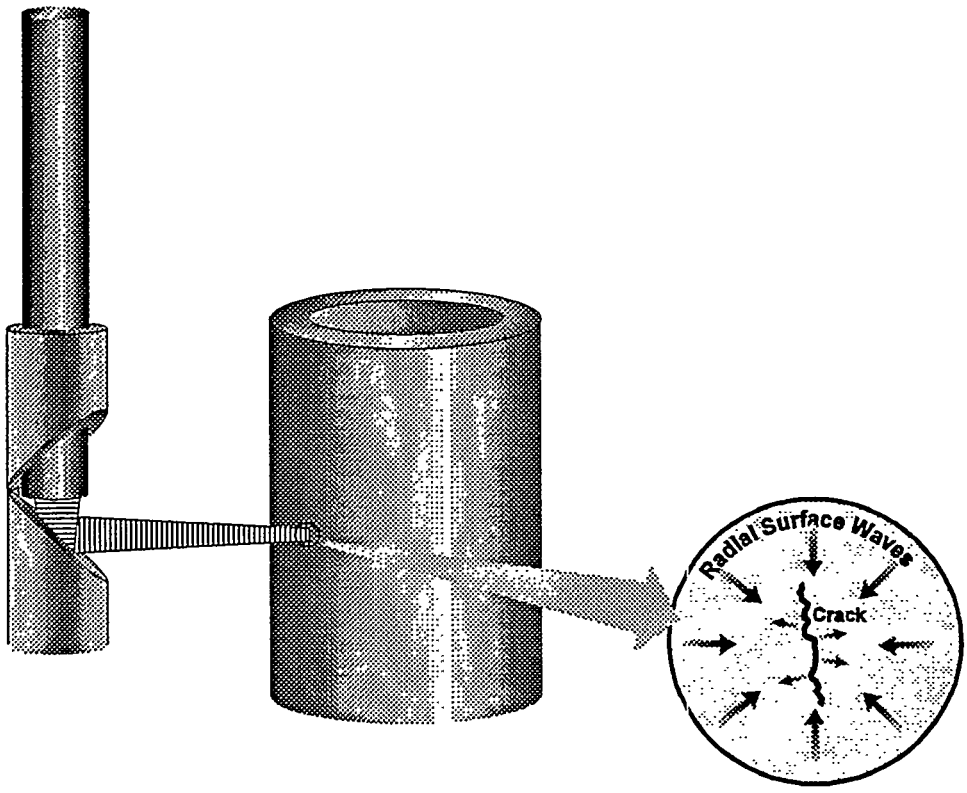

Figure 2. Setup for Radial Surface Wave Inspection of Aluminum Oxide Tubes

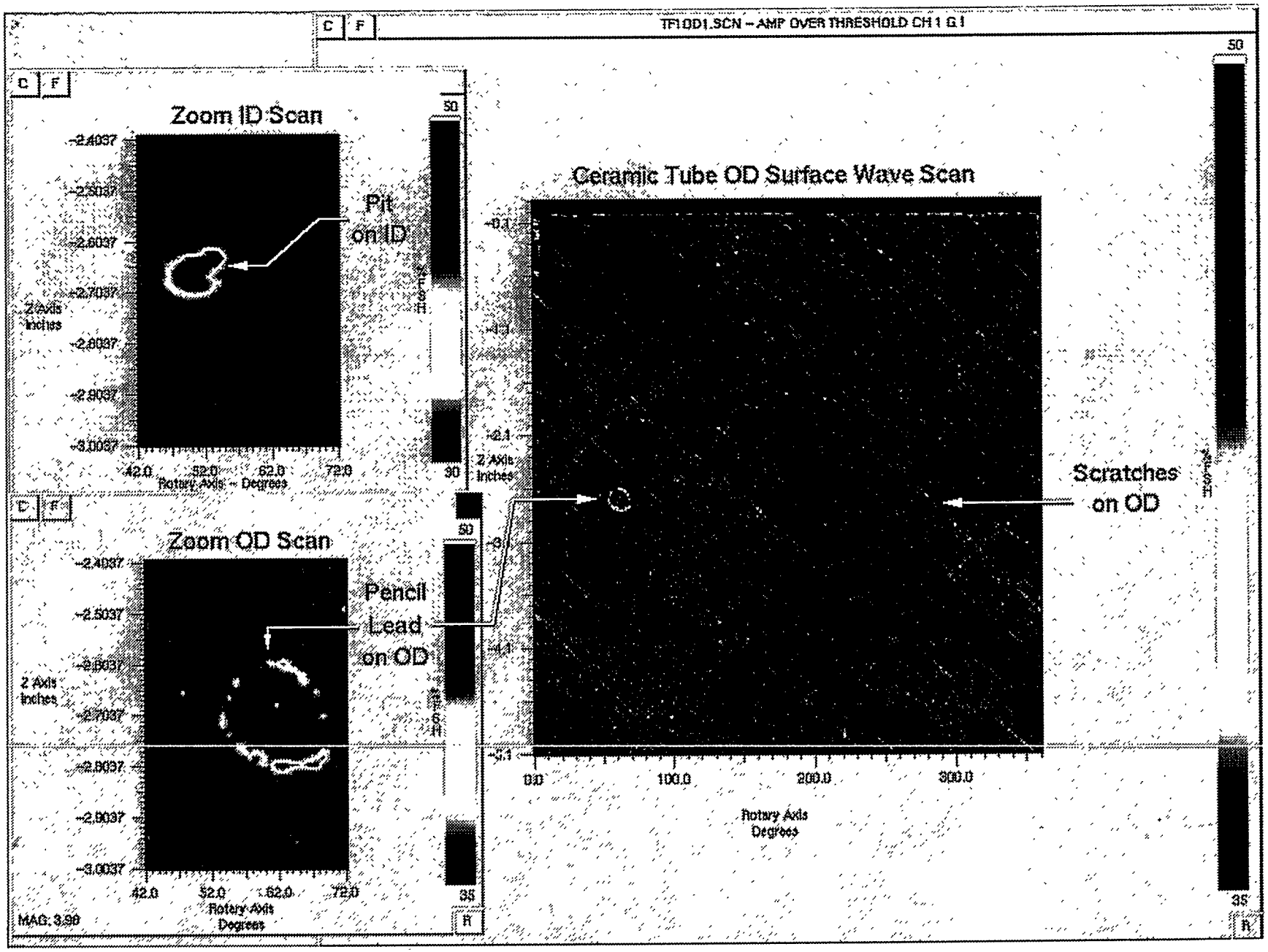

Figure 3. Ultrasonic Radial Surface Wave Inspection of Aluminum Oxide Tube F1 with ID Surface Pit

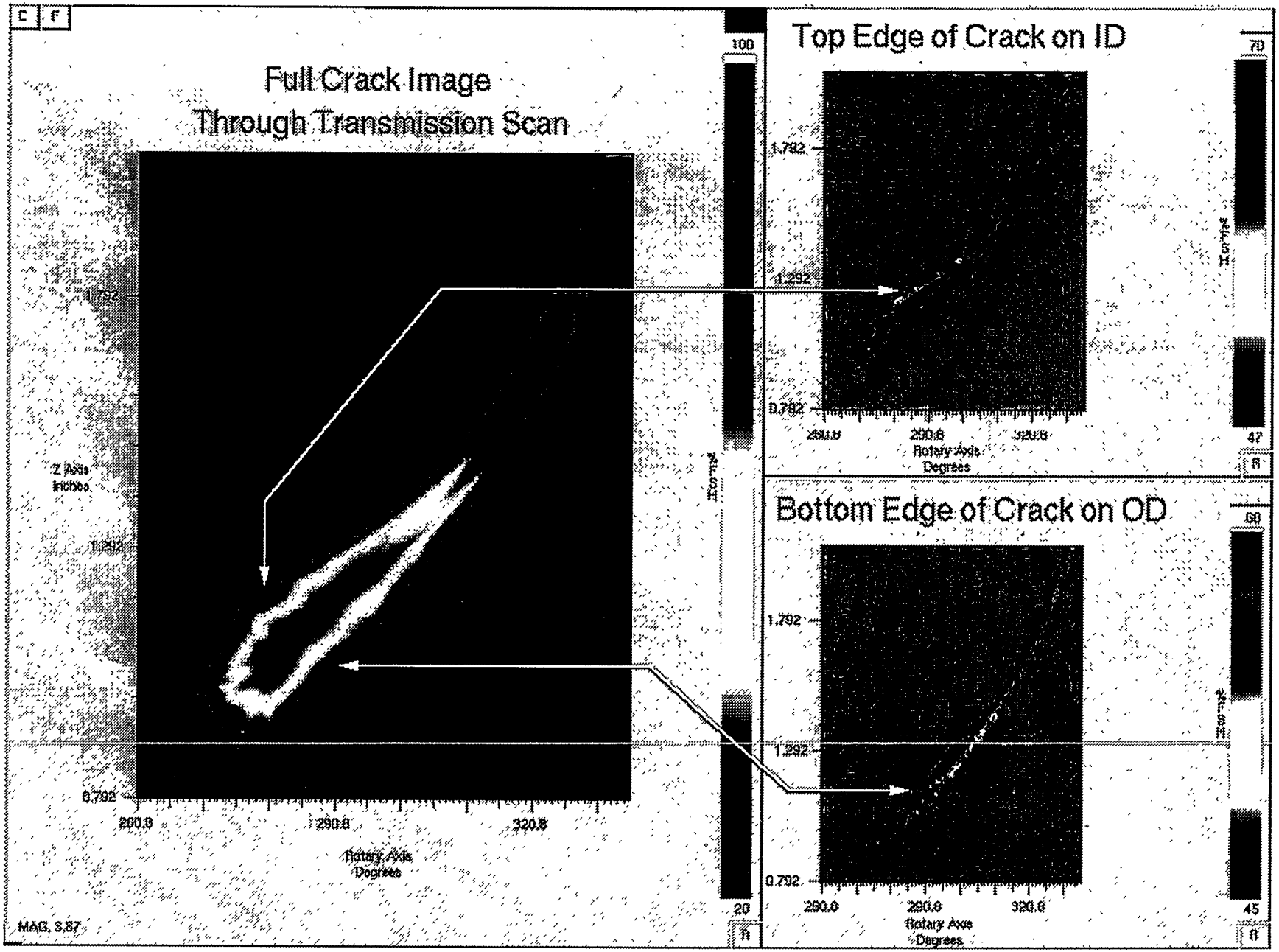

Figure 4. Through Transmission Image of Crack in Aluminum Oxide Tube T1

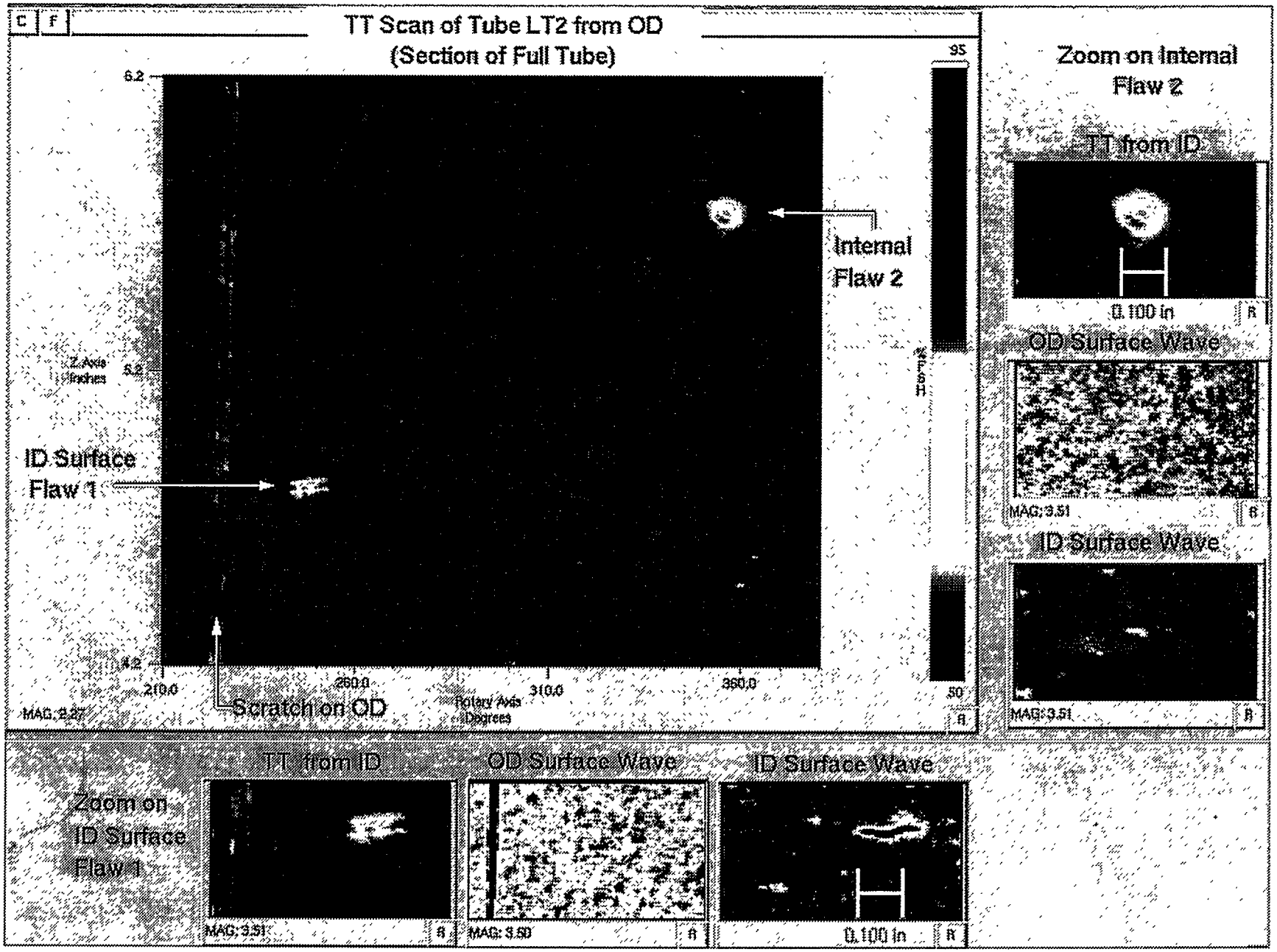

Figure 5. Through Transmission Image of Internal Flaw in Aluminum Oxide Tube LT2

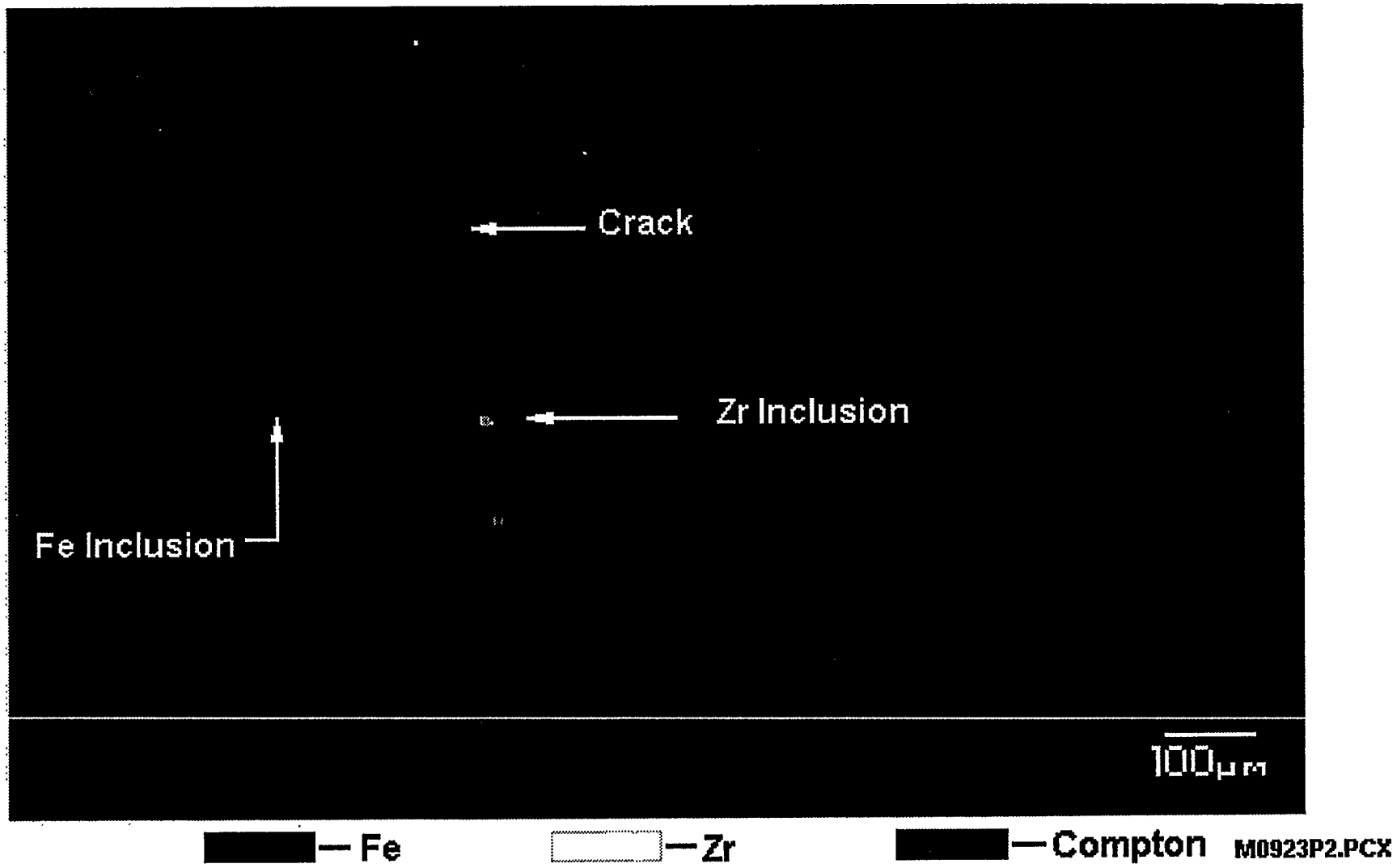

Figure 6. X-Ray Microfluorescence Image of Zirconium Inclusions in a Crack in Aluminum Oxide Tube T1.

with a majority of grains in the 5 to 10 μm range and a second group of grains in the 30 - 50 μm range. Figure 7 shows the microstructure of three of these samples. The velocities observed are shown in Table II. The velocity difference between samples was calculated using the fine-grain high density sample 998-5 as a reference and is shown as a percent difference. Note that there is essentially no difference between the two fine-grain high density samples but that high density sample with the dual population of grains and the low density sample can be separated from the fine grain samples by a simple velocity measurement. The velocity measurement appears to be sensitive to the measurement of sample structure of these specimens. Velocity measurements were also made of several other samples supplied by the industrial partner. A small wafer was removed from each sample and broken to expose a fracture surface for scanning electron microscope (SEM) inspection. There were two groups of samples. The first group (samples L1-L5) consisted of samples that apparently were not fully sintered. With the exception of sample L4, these samples had varying amounts of small relatively smooth grains in the 2-10 μm size range. The failure mode was by intergranular fracture. Some samples had a larger second population of grains. There was also some indication of 100-150 μm agglomerates of the small grains in several samples. Sample L4 failed by transgranular fracture and had irregular grains in the 20-40 μm size range. The second set of samples (S4-S5) failed by transgranular fracture and had irregular grains in the 5-15 μm range. Table III summarizes the velocity and SEM data obtained from these samples. In general, the full density samples with larger grain size have higher velocities.

Table II - Ultrasonic Velocities Measured in Aluminum Oxide Specimens

Three-Point Bend Samples	Longitudinal Velocity (in/μs)	% Diff	Shear Velocity (in/μs)	% Diff	Density (gm/cm^3)
998-5 (small grains)	0.4063 +/- 0.0007		0.2436 +/- 0.00005		3.90
998-10 (small grains)	0.4063 +/- 0.0007	0.01%	0.2436 +/- 0.00005	0.06%	3.90
998-8 (dual phase)	0.4178 +/- 0.0007	2.82%	0.2481 +/- 0.00005	2.32%	3.90
940-14 (larger grains, porosity)	0.3811 +/- 0.0006	-6.21%	0.2283 +/- 0.00005	-6.26%	3.62

Resonant Ultrasonic Spectroscopy

The Resonant Ultrasonic Spectroscopy (RUS) technique excites a sample using a swept frequency oscillator and listens for resonances within a part. For a well defined part geometry, a series of sharp resonant peaks are obtained. If there are defects within the part some of these resonant peaks may be split enabling the technique to quickly identify parts with defects. In order to use the RUS technique a sample is excited with a swept frequency transmitter. This excitation will cause the sample to vibrate in each of its resonant modes. By using one or two sensitive tuned receivers, the vibration of the sample may be detected. The vibration frequencies are primarily determined by the sample geometry and material properties. The number of excited frequencies can be very large except for the most simple of geometries. In addition, it is difficult to determine the vibration mode that belongs to each frequency. In general, a vibration analysis of the part geometry should be used to identify the vibrational modes of the detected frequency resonances. We have used a finite element analysis to calculate the vibrational modes of tubes.

If a resonant frequency analysis is not available, the technique may still be used if inspecting a number of identical parts. The resonance spectrum of a good part may be used as a baseline to be compared with spectra from the rest of the parts. Changes in the spectra may be indicative of defects within a part.

The frequency resonances are dependent upon the sample geometry, the variation in sample dimensions, the material properties and the presence of defects within the sample. Small dimensional and material property differences between samples will cause some of the resonant frequencies to broaden, split or change frequency between samples. Defects within a sample will cause resonant frequencies to broaden or split.

Sample 998-5
Density 99.8%
Small Grains

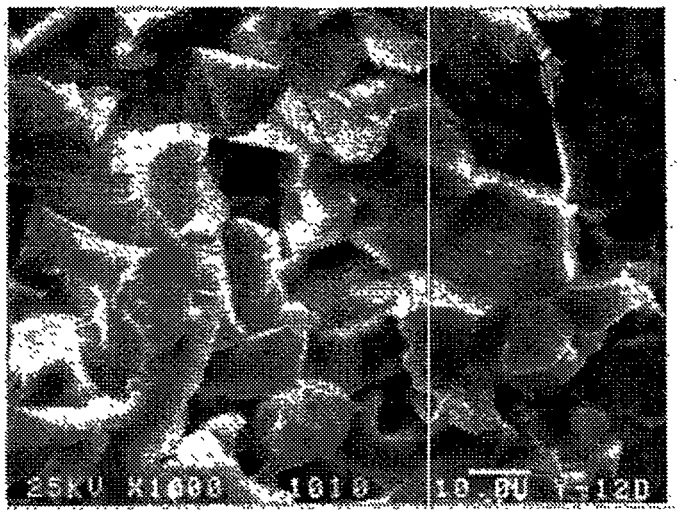

Sample 998-8
Density 99.8%
Dual phase

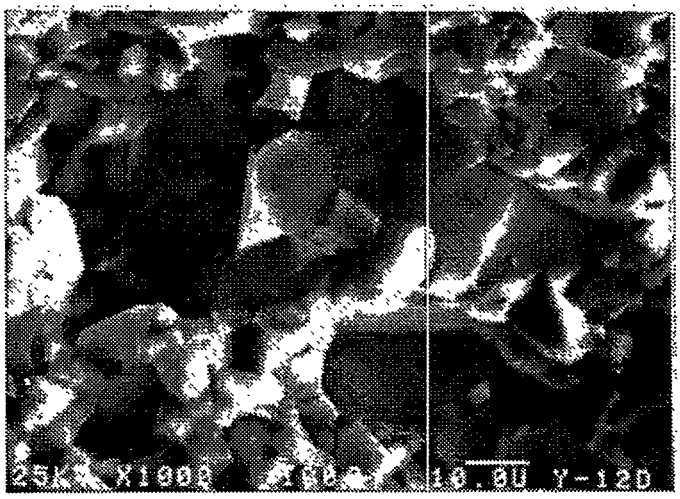

Sample 940-14
Density 94.0%
Larger Grains
Porosity

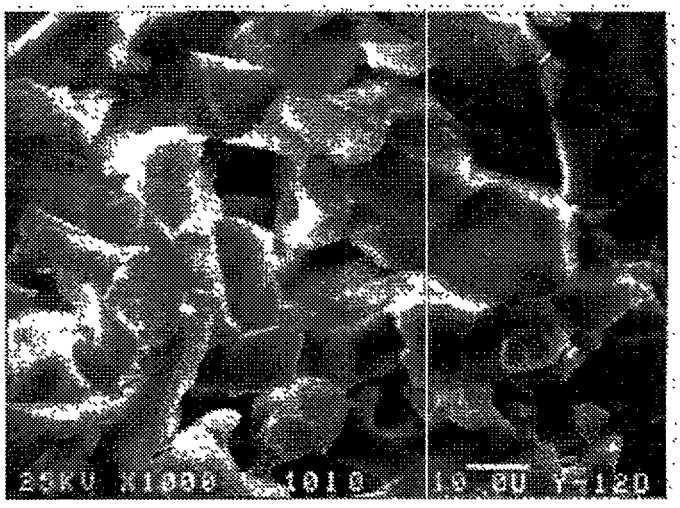

Figure 7. SEM Microstructure of Three-Point Bend Samples.

Table III - Summary of SEM and Velocity Data on Aluminum Oxide Samples

Sample ID	SEM Results	Longitudinal Velocity	Shear Velocity
998-5	5-10 μm irregular grains with isolated fractured grains to 20 μm. Intergranular fracture, Some bonding between grains.	0.4063	0.2436
998-8	Dual phase, 5-10 μm grains and 30-50 μm fractured grains. Some bonding between grains. Transgranular fracture.	0.4178	0.2481
998-10	5-10 μm irregular grains with isolated fractured grains to 20 μm. Intergranular fracture, Some bonding between grains.	0.4063	0.2436
940-14	15-25 μm grains with 10-15 μm porosity. Grains bonded together, Transgranular fracture.	0.3811	0.2283
L1	Spherical agglomerates of grains ~150 μm dia. Dual phase, 5-10 μm and 25-40 μm smooth grains. Has several spheres 600 μm dia with 40-70 μm grains that may be shells and "worm tracks" near edge. There is a remnant structure that may be from a 900 μm dia spherical shell. Some bonding between grains. Intergranular fracture.	0.4301	0.2553
L2	Dual phase with 30-80 μm and 5-20 μm grains. Little apparent bonding between grains. Intergranular fracture except in cleavage fracture near edge.	0.4295	0.2554
L3	Multisided agglomerates of grains 100-200 μm dia. Agglomerates made up of 2-10 μm smooth grains. Some areas have some melting together of small grains into 10-20 μm clumps. Some bonding between grains. Intergranular fracture.	0.4232	0.254
L4	20-40 μm irregular grains. Grains bonded together. Transgranular fracture.	0.4272	0.254
L5	2-10 μm smooth grains. Some indication of 100-200 μm agglomerates. Not as evident as in L3. Intergranular fracture.	0.428	0.2539
S4	5-15 μm irregular grains. Grains bonded together. Transgranular fracture. Some areas with grains to 40 μm.	0.425	0.2518
S5	5-15 μm irregular grains with uniform scattering of 30-50 μm grains. Grains bonded together. Cross granular fracture.	0.4248	0.2521

The difficulty with long (>6 inches) aluminum oxide tubes is determining which mode belongs to which resonant frequency. The tube geometry is fairly complex with modes that are determined not only by the sample length, but also by the sample diameter, concentricity and wall thickness. In addition, no two tubes have identical dimensions. At this time, we have not been able to separate the frequency shifts and splits caused by dimensional variations from the resonant frequency splits caused by actual defects within a tube. We have had success with the shorter ring tensile specimens used in Phase II to evaluate the strength of the tubes. These data are presented later in this report.

Analysis of NDE Techniques

Table I shows the NDE inspection techniques used on each sample. The sample conditions shown were determined either by visual inspection or by SEM analysis. Also shown are the techniques used that were able to detect the known sample conditions.

The thermal inspection techniques were found to be insensitive to small defects in aluminum oxide samples. It appears that the high thermal conductivity of the material causes the rapid dispersion of heat within a sample which prevents the system from detecting defects within a sample.

Radiographic techniques can detect small pits and voids but not with the same resolution as ultrasonic techniques. In addition, radiography is insensitive to closed cracks.

The X-ray microfluoroescence inspection is useful for evaluating material composition in the vicinity of a defect. Although not viable for general inspection of full tubes, this technique can be useful for determining the cause of a specific defect.

Ultrasonic inspection techniques have been the most successful for inspecting the aluminum oxide tubes from the industrial partner. It appears that a combined inspection including both a through transmission and a pair of surface wave inspections would be capable of detecting small internal and surface cracks/defects. The through transmission scan is necessary to detect internal voids, inclusions, and cracks. The surface wave inspection will detect surface and near surface defects. Since the inside surface is probably the most critical, it may be possible to eliminate the outside surface wave inspection. Ultrasonic inspection equipment is available that can take on the order of 5000 points per second. To obtain adequate resolution, the tubes should be scanned with a resolution of 0.010 to 0.015 inch. With this range of resolution, a tube can be scanned at 3 to 7 inches of tube per minute.

Acoustic velocity measurements have been shown to be sensitive to material processing parameters. The three-point bend samples were produced under closely controlled conditions. The differences between samples with different processing conditions was easy to detect. There was greater difficulty detecting differences in the aluminum oxide samples obtained from the industrial partner. Although there was significant differences in the sample structure, there was little difference in ultrasonic velocity between samples although larger grain sized samples had higher velocities. It is obvious that more work would be necessary to relate specific material variations to changes in velocity. This effort is beyond the scope of this work.

The resonant ultrasonic spectroscopy technique has promise for inspecting small uniform parts. The technique relies on being able to choose several resonant frequency modes in a sample that would be modified by the presence of defects in the sample. In order to make the best use of the system, dimensional variations between parts must be minimized. The dimensions of the tubes (in particular, wall thickness and OD surface roughness) were not well controlled, causing frequency shifts and splits that could not be correlated with the presence or absence of defects in a sample. Since no two tubes were alike, we were not able to establish a baseline set of frequencies to be used to compare good and flawed tubes. In the Phase II study we had a number of identical samples from each tube. Thus, the RUS technique was used for the Phase II study.

PHASE II EFFORTS

The Phase II effort involved the fabrication of three tubes for nondestructive and destructive evaluation. The plan was to fabricate one tube using standard fabrication techniques. A second tube would be overfired to produce grain growth in the tube microstructure, and the third tube would be a defective tube with flaws. Once the tubes were fabricated, they would be inspected using the ultrasonic inspection techniques developed in Phase I and cut into 1 inch long ring tensile specimens. The ring tensile specimens would be evaluated using the RUS inspection and then tested to failure. The failure load data would then be analyzed using Weibull statistics.

Tube Fabrication

A significant effort was required to fabricate the three tubes. In the first effort, the unflawed and the overheated tube were cracked. The supposed defective tube contained only benign outside surface irregularities. A second set of tubes were fabricated. In the second set, a 54-inch long tube that was thought to represent good product was found to have extensive microcracking on the tube ID. This tube was chosen to represent a defective material condition. It took three tries to make an overfired tube that did not break. After the three suitable tubes were obtained for the Phase II study, they were cut into three equal sections to fit into our fixturing and inspected using ultrasonic techniques.

Ultrasonic Inspection

Ultrasonic inspection was performed on all three sets of tubes. Radial surface wave inspections of both the inside and the outside surfaces as well as a through transmission were made. Figure 8 shows the radial surface wave inspection of the inside surface of one of the sections of the tube that had microcracks. The microcracks are clearly visible. The variation in shading in the scan is due to a misalignment in the scan setup. The tubes are fabricated by forming the aluminum oxide on a steel rod. The tube is pushed off of the rod and then fired in a furnace. The microcracking condition was apparently caused by damage to the tube when it was removed from the steel rod before firing. The microcracks were not detected by the dye penetrant inspection performed by the vendor.

Resonant Ultrasonic Spectroscopy (RUS)

Since we have a large number of nearly identical samples, we thought that RUS inspection would be a valuable tool to detect differences between tubes. In order to prepare for the RUS inspection, a finite element analysis (FEA) model was used to calculate the expected vibrational modes in an aluminum oxide tube of the same dimensions as the ring tensile specimens. Figures 9-11 show selected resonant modes for the ring tensile specimens. For some of the modes shapes, two mode numbers are given. In these cases, the modes only differ in orientation. Modes 1-6 are tilt modes with no distortion of the tube and are not shown. The color indicates relative displacement. In Figures 9-11 distortion is greatly exaggerated. Several characteristic mode shapes can be identified. The first set of modes involves a circumferential resonance which is characterized by modes 7,8,11,12, 15,16, 25,26, etc. A similar set of modes involves both circumferential and axial resonance and is characterized by modes 9,10,13,14,19,20, etc. A tilting set of modes is seen in modes 17,18, 28,29, etc. Hoop modes are seen in modes 21, 27 and 55. Axial longitudinal modes are seen in modes 22 and 82. A torsional mode is seen in mode 44.

After the FEA model was completed, the ring tensile specimens were tested using the RUS technique. A set of characteristic frequency peaks were obtained for each tube. Figure 12 shows a typical set of resonances. The peaks obtained in the range of 10 to 160 kHz for all the specimens are plotted in Figures 13 and 14. The vertical axis represents the location of each specimen within its respective tube (note that the overfired tube is offset by 40 inches and the flawed tube is offset by 80 inches to get the data from all three tubes on the same

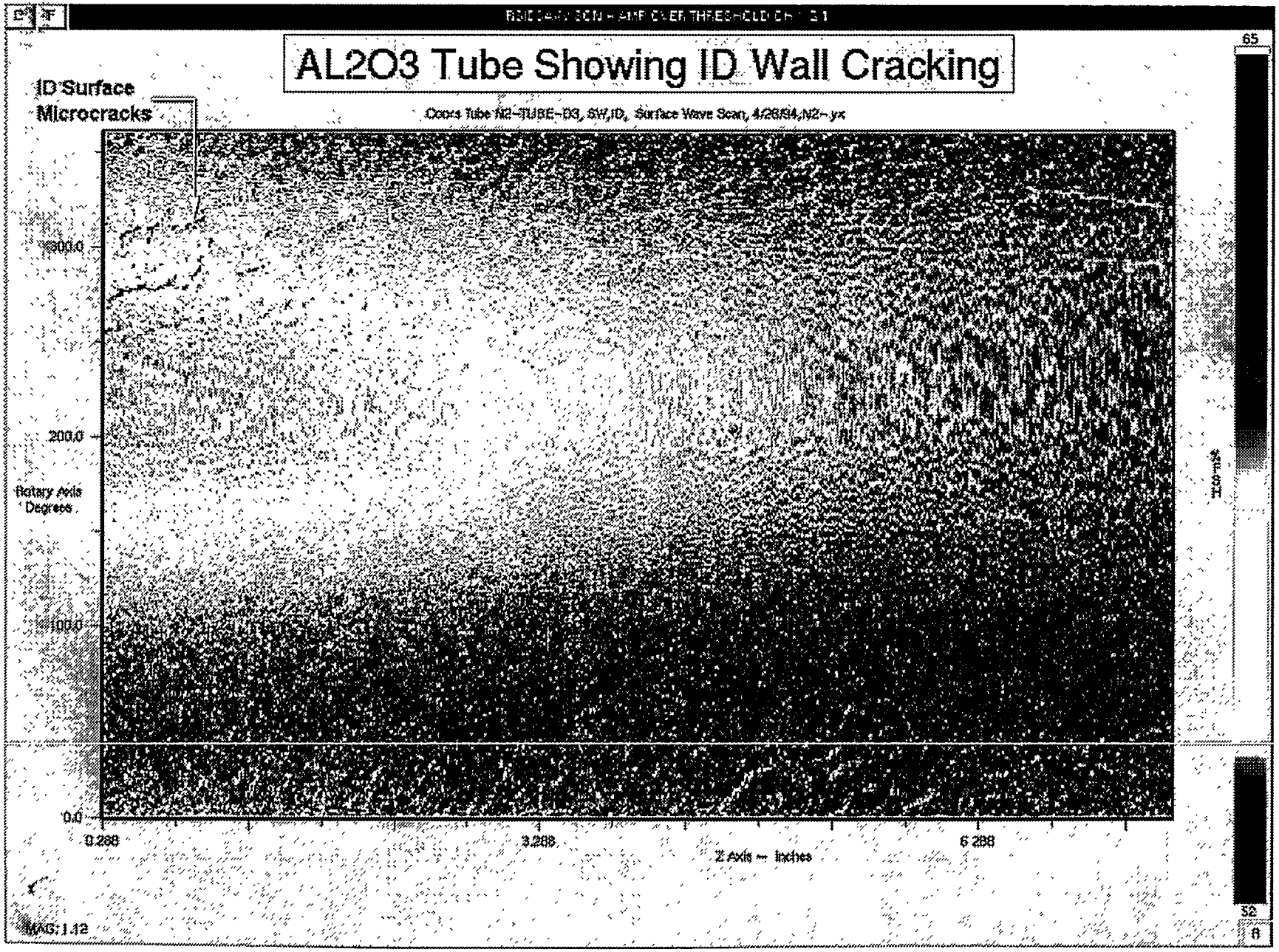

Figure 8. Radial Surface Wave Inspection of ID Surface of Tube With ID Microcracks

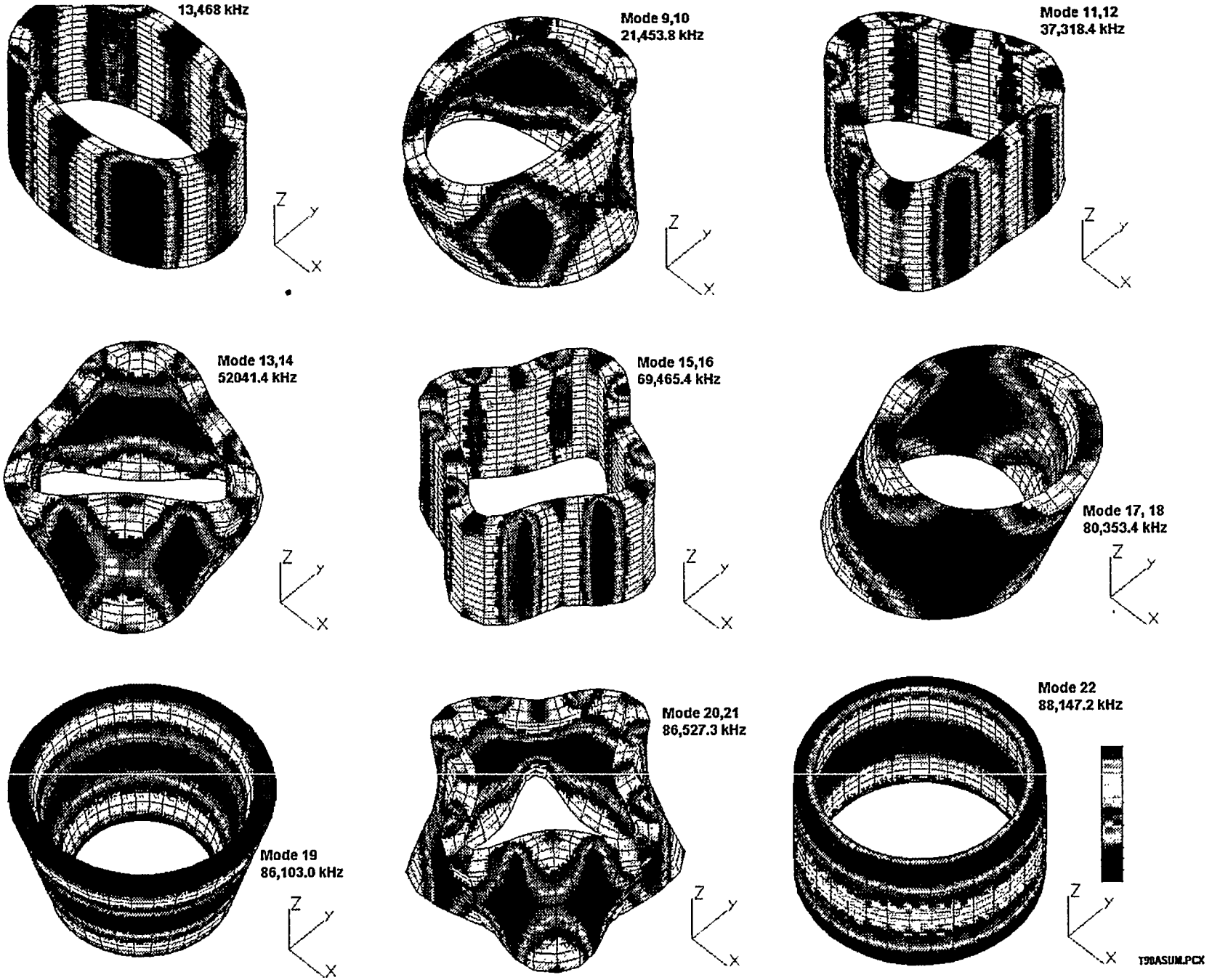

Figure 9. Resonant Modes 7-22 for 0.900-inch long Aluminum Oxide Tube

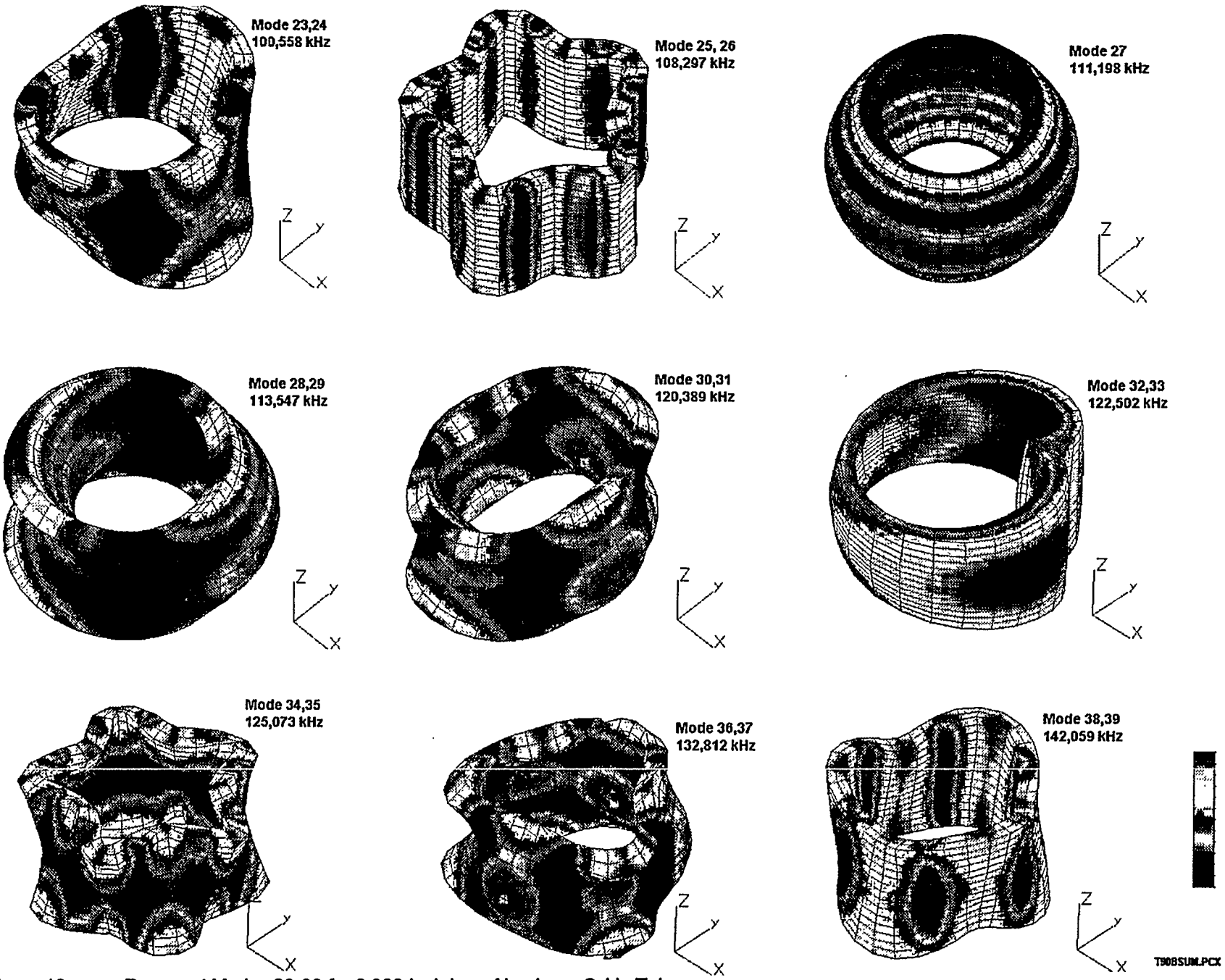

Figure 10. Resonant Modes 23-39 for 0.900-inch long Aluminum Oxide Tube

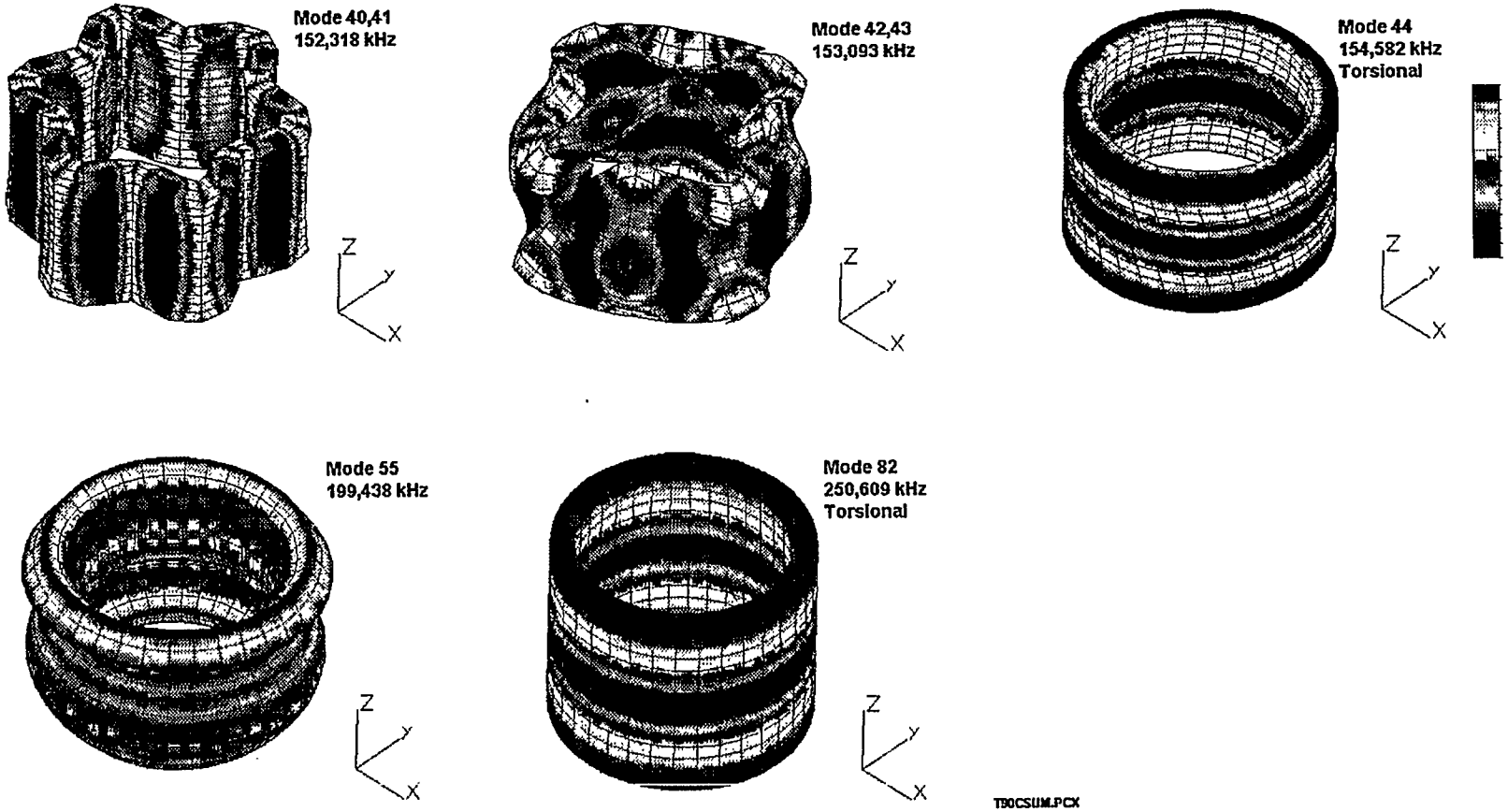

Figure 11. Resonant Modes 40-44,55, and 82 for 0.900-inch long Aluminum Oxide Tube

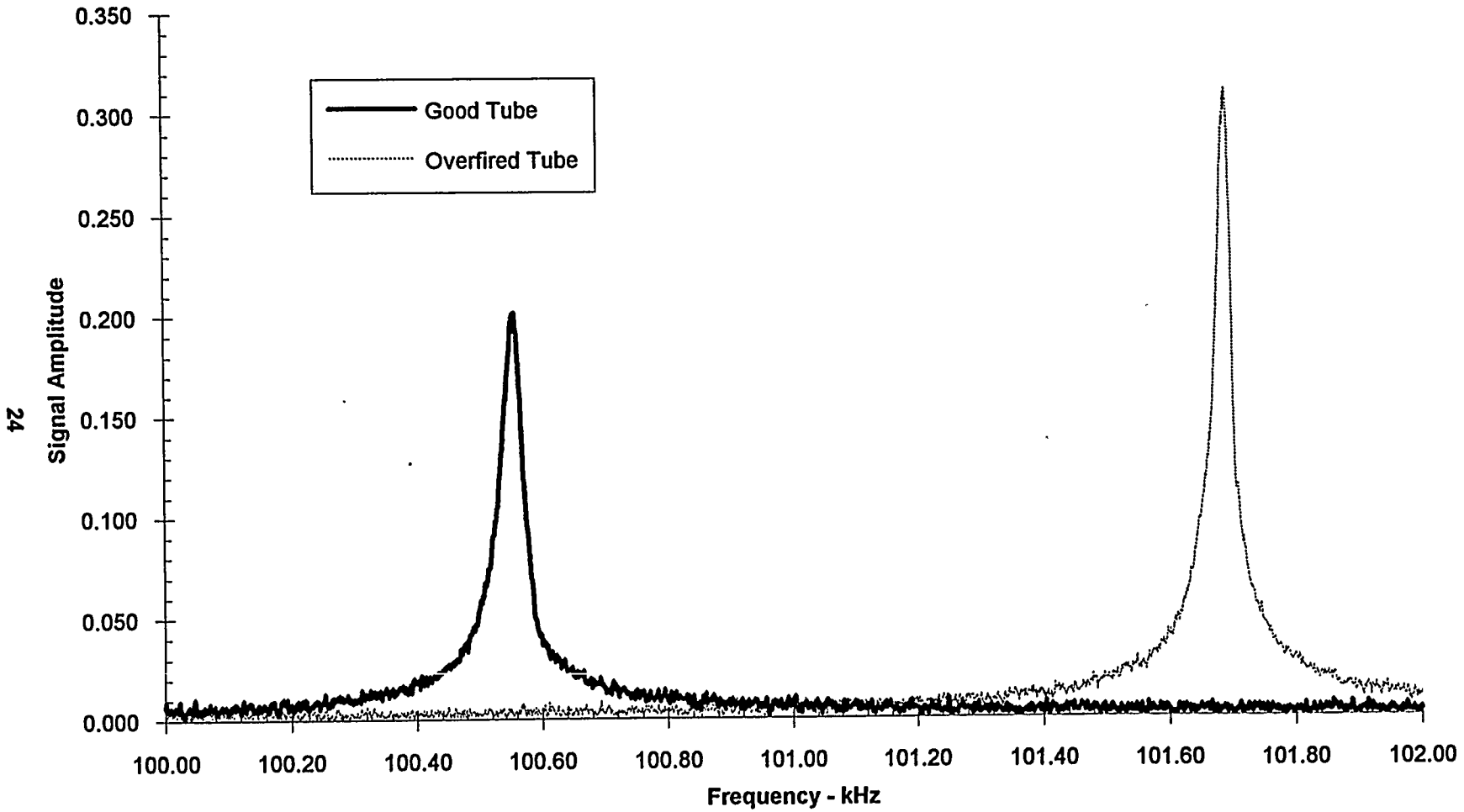

Figure 12. Typical Set of Resonant Peaks for Aluminum Oxide Ring Tensile Specimen.

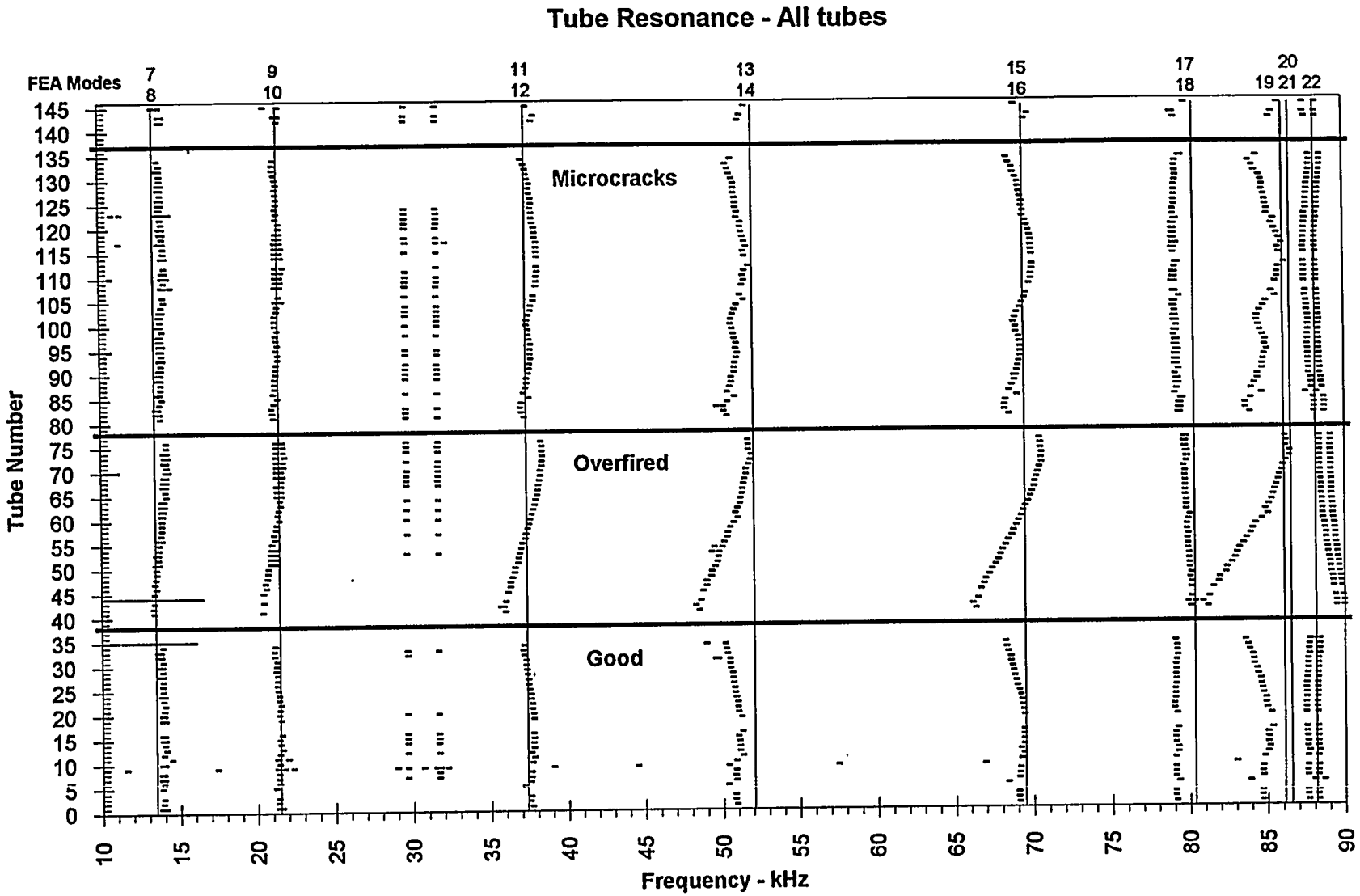

Figure 13. Resonant Peaks Between 10 and 90 kHz for All Ring Tensile Specimens.

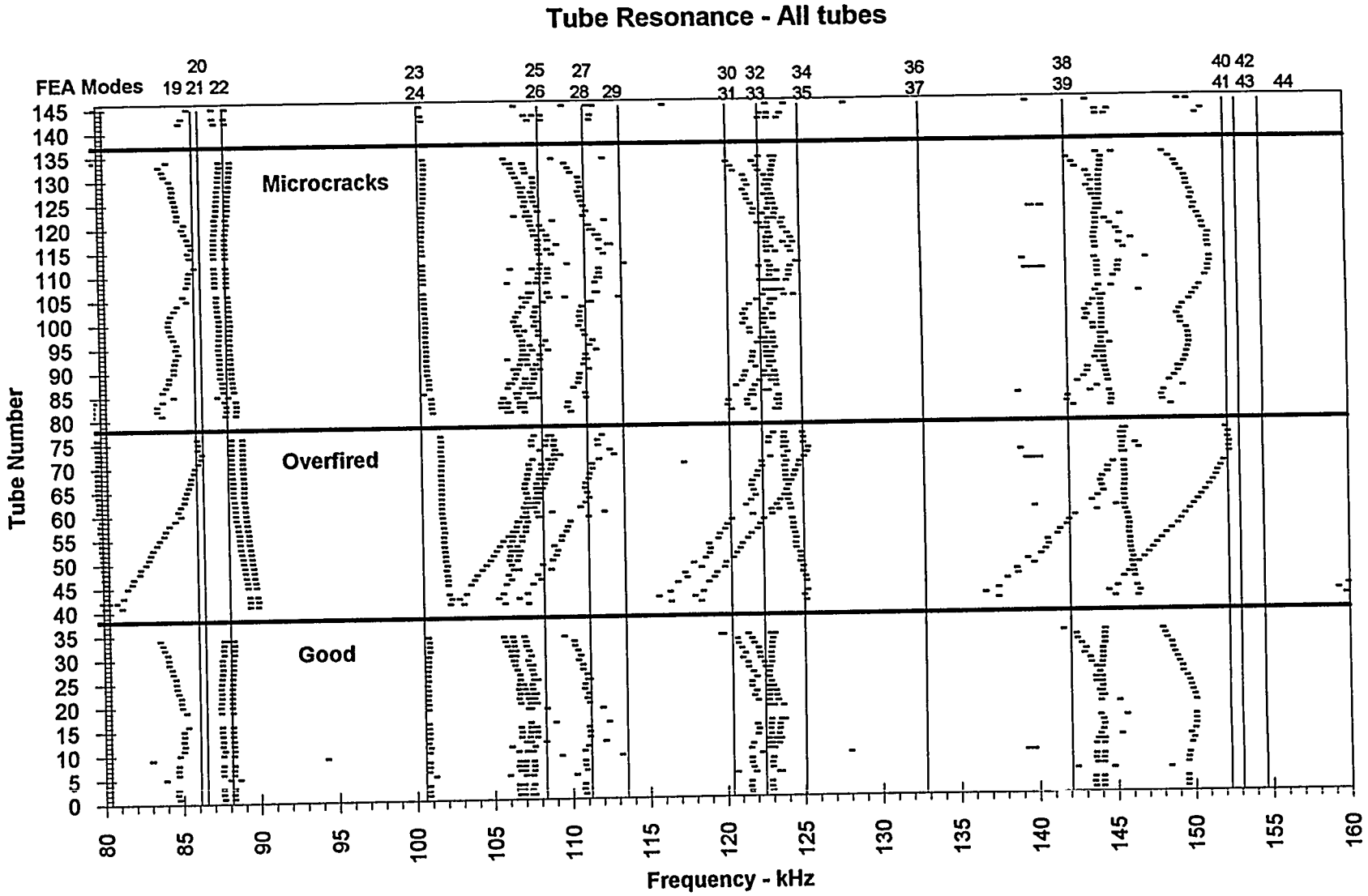

ALL180.XLC 11/22/94

Figure 14. Resonant Peaks Between 80 and 160 kHz for All Ring Tensile Specimens.

plot). The horizontal axis represents frequency and the points are plotted at the resonant peak location. Vertical lines are drawn at each frequency were the FEA calculation predicts a resonant mode. The mode numbers are listed at the top of each line and correspond to the resonant modes displayed in Figures 9-11. The resonant frequency is reasonably uniform over the length of the good tube. There is a significant variation in resonant frequency for over the length of the tube for the overfired tube particularly for those frequencies that involve a circumferential resonance. The frequency shift is not as evident in modes 17, 18 (tilt), mode 22 (longitudinal) and modes 23,24 (mixed). The magnitude of the frequency shift increases with mode number. Similarly for the tube with microcracks there is a characteristic pattern of frequency shift along the length of the tube. Figure 15 shows an expansion of resonant modes 23 and 24 near 100 kHz. These modes appear to contain circumferential shear and axial modes. For these modes, the good tube produces a constant frequency near 100.6 kHz. The overfired tube produces significantly higher frequencies and the microcracked tube also shows a frequency increase except for one location approximately 35 inches from one end of the tube. This resonance can be used to separate the different tubes. Several of the ring samples were mislabeled. By using the RUS inspection and markings on the tubes, we were able to identify the tube and the location of these ring specimens.

Ring Tensile Test

The strength of a group of brittle ceramic specimens will vary due to the presence, size, and location of flaws in the material. All materials have flaws at least on the microstructure level. Thus for a sample consisting of several identical specimens, there will be a range of strengths depending upon the population and distribution of flaws within the sample specimens. The upper limit on strength is determined by the microstructure of the sample. Weibull statistics are used to evaluate the data. The ring tensile test is designed to determine the failure strength of brittle materials. A tubular specimen is placed between two hold down plates that are loaded against a one-inch high spacing ring that prevents the plates from loading the ends of the tube. A rubber bladder is placed inside the specimen and pressurized. This places a hoop stress on the sample. The bladder is pressurized until the specimen fails and the failure pressure is recorded. The failure strength (or stress) can then be calculated. If a strain gage is mounted on the specimen, Young's modulus can be measured. The tube must be long enough so that the bladder does not extrude into the gap between the tube and the hold down plates.

The rubber bladders had to be fabricated specifically for this test. We were able to find fixturing to fabricate rubber bladders for ring tensile test with only minor modification.

Due to a fabrication mistake, most of the specimen blanks were too short to fabricate the one-inch long specimens. It was necessary to finish grind the specimens to a length of 0.900 inches to obtain equal length specimens. We had to fabricate a special shim washer with a hole in the center to fill in the 0.100-inch gap between the specimen and the hold down plates in order to accommodate the shorter specimen length and the rubber bladder. The setup is shown in Figure 16. The strength of the specimens is relatively independent of small changes in the specimen length. In longer specimens there is a higher probability of there being a larger flaw present, and hence lower strength.

Weibull Statistical Analysis[1]

If a single test result corresponds to a single-strength specimen outcome, then a group of specimens, all tested under identical procedure represents a sample. The true distribution parameters for all specimens are defined as the population parameters. From the sample, it is possible to estimate the population parameters, but there will generally be some variability in the sample estimates due to inherent statistical fluctuations. In order to perform the Weibull analysis, the specimen strengths are ranked in order and assigned a probability. The data are then graphed where the abscissa is the natural log of stress, and the ordinate is the cumulative probability of failure in percent. Figure 17 shows the data from the ring tensile tests. The actual stress and the calculated probability values are shown on the axes for convenience. A simple least squares regression line is applied to each data sample. The Weibull modulus is the slope of the sample. The characteristic strength of each

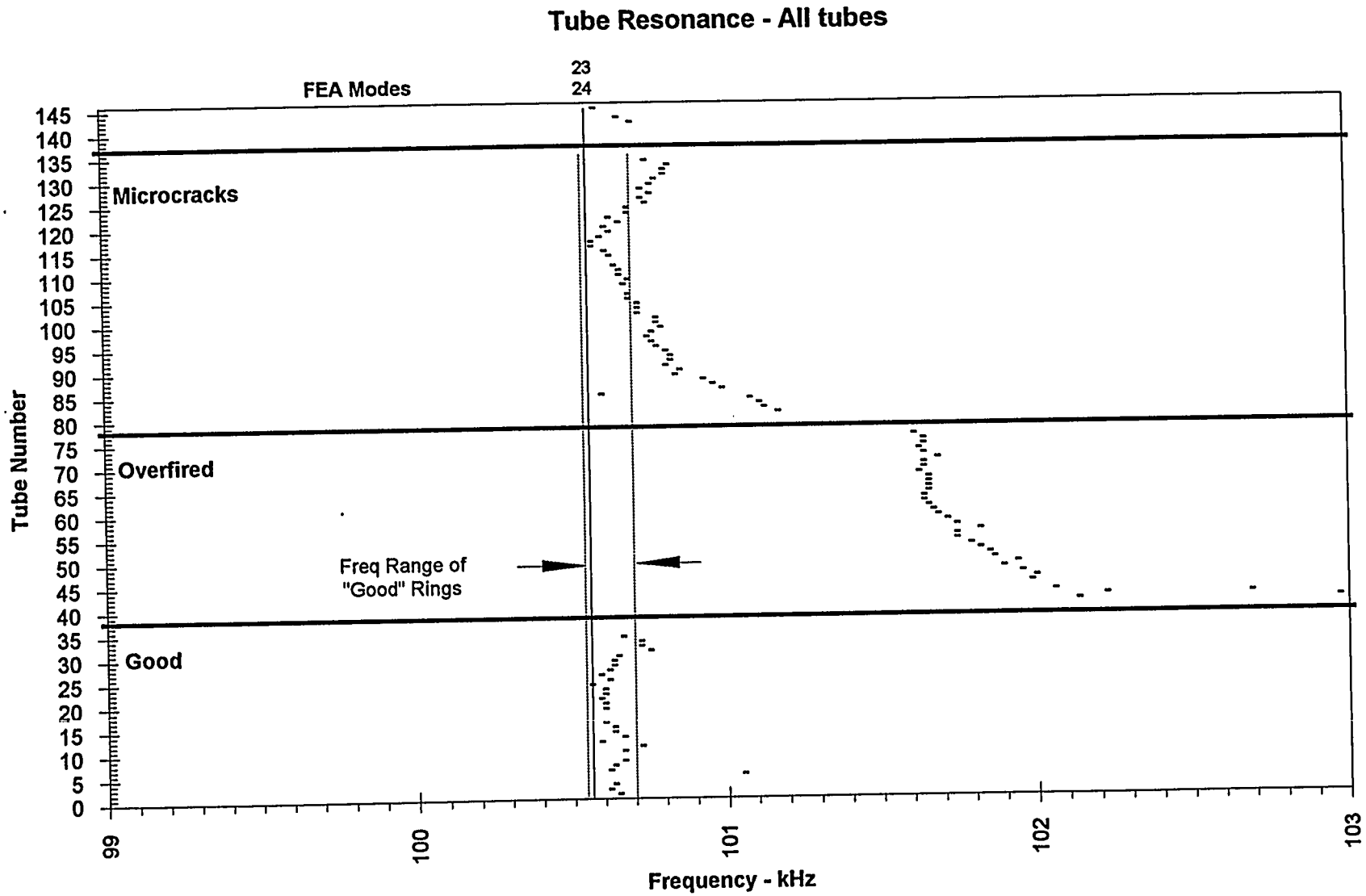

Figure 15. Resonant Peaks Near 101 kHz for All Ring Tensile Specimens.

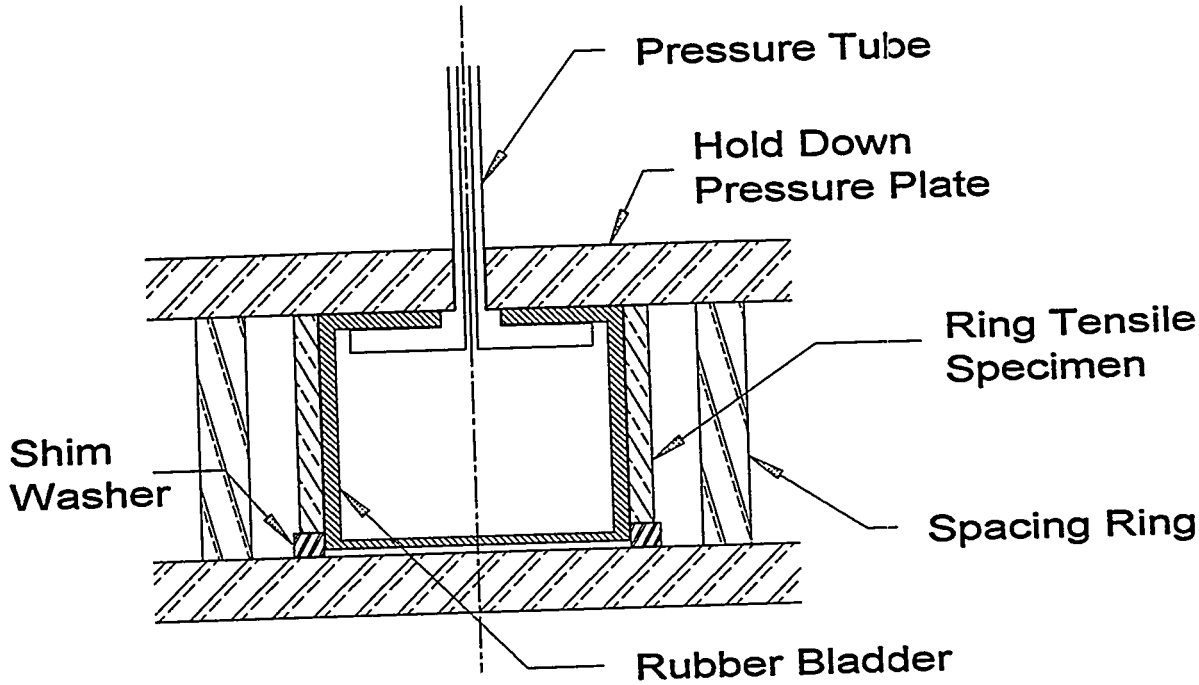

Figure 16. Setup for Ring Tensile Test.

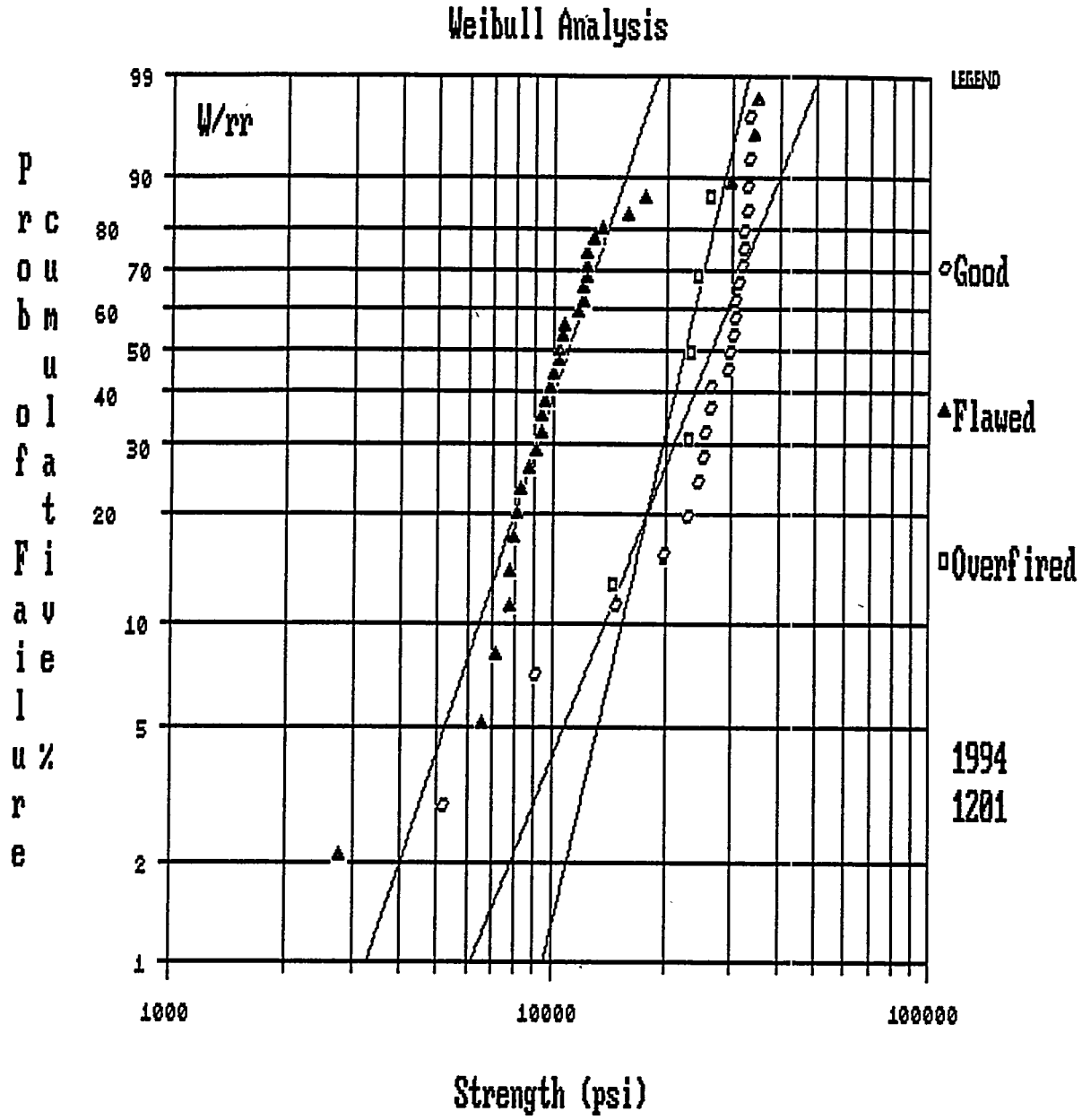

Figure 17. Weibull Analysis of Ring Tensile Data

sample corresponds to the 63.2% probability of failure. The Weibull modulus thus is an indicator of population variability and the characteristic strength a convenient indicator of strength.

Three samples are plotted in Figure 17. The circles represent the strengths obtained from the specimens of the good sample. The characteristic strength is 32.1 ksi. The lowest (weakest) four specimens deviate from the linear fit and may be due to defects in critical locations for these specimens. The triangles represent the strengths obtained from the specimens of the sample with microcracks. It is interesting that there are four "strong" specimens that overlay the data from the good sample. The remaining specimens of the microcracked sample fall on a curve with a characteristic strength of 12.1 ksi. This indicates that the majority of the tube had microcracks in critical locations that weakened the tube. The highest stress in a ring tensile test is on the ring ID and thus, microcracks on the tube ID would have the greatest tendency to reduce the strength of the specimen. The four high strength specimens apparently had no microcracks in critical areas of the specimen so that the strength was determined by flaws of a smaller size, limited by the material microstructure. Only five of the specimens from the overfired tube could be tested. These data are plotted as squares. These specimens appear to have a strength on the order of 24 ksi, intermediate between the good and the overfired samples. Five specimens are not enough to obtain adequate statistics on the strength data from a sample. Thus we can only say that the overfired sample may have a strength between the good and the microcracked sample.

CONCLUSIONS

This CRADA has been beneficial for both DOE and the industrial partner. The initial survey of inspection techniques identified viable techniques for inspecting the aluminum oxide tubes. Radiographic techniques were useful for detecting pits and voids and inclusions. An x-ray microfluorescence technique using an x-ray microprobe was useful in identifying small inclusions. This is a useful technique for diagnostics but unsuitable for general production inspection. Acoustic techniques showed the greatest promise for tube inspection.

The strength of the tubes are dependent upon the absence of critical defects. In order to detect surface and near surface defects on this wall, a radial surface wave inspection was developed that is insensitive to the orientation of the defect. This technique has been successful in detecting microcracks, pits, surface perturbations, and even the presence of graphite (pencil lead) markings on the tube.

Ultrasonic velocity measurements have been shown to be sensitive to material processing variations that result in density and grain size variations. Further study of a controlled series of samples is necessary to develop a correlation of velocity to material processing parameters. The difficulty in producing these samples by the industrial partner and the emphasis on determining tube strength put this study beyond the scope of the CRADA.

Resonant ultrasonic spectroscopy measurements were useful for the ring tensile specimens. Variation in material properties along the length of the overfired tube were readily evident. Differences were detected by frequency shifts of selected resonant modes. We were also able to detect differences between the good and the microcracked tubes. The RUS measurements were not usable on full length tubes. The material property variations between full length tubes were overshadowed by the dimensional differences between the tubes. The RUS inspection has shown promise for detecting differences between shorter specimens with identical geometries and may be useful for other part geometries produced by the industrial partner.

The ring tensile testing showed the differences in tube strength. The microcracked tube was produced using normal production parameters and was intended to be a good tube. Damage to the tube when it was handled before firing produced the microcracks. The significant weakening of the tube caused by the microcracks shows the importance of being able to detect this condition. The microcracks were detected using the radial surface wave scan on the tube ID. An operational stand down at Y-12 prevented the complete testing of the overfired tube. Thus, only five ring tensile specimens from the tube were tested and the data are incomplete. However, it can be seen that the strength of this tube may fall between the strengths of the good and the microcracked tube.

The most important effect on tube strength is the presence of critical defects. Microcracks on the tube ID have been shown to significantly weaken the tube. We were able to develop a test that is able to detect this condition. It is recommended that an ultrasonic inspection be implemented to detect tube defects.

REFERENCES

1. George D. Quinn, "Flexure Strength of Advanced Ceramics - A Round Robin Exercise," MTL TR 89-62, U.S. Army Materials Technology Laboratory, July 1989.

Distribution:

Coors Technical Ceramics Company, Oak Ridge, TN

John Ghinazzi (10)

Oak Ridge Y-12 Plant

T. W. Dews
G. W. Joe
A. K. Lee/OSTI (2)
M. W. Moyer (5)
S. G. Snow/K. A. Kitzke
R. S. Steele
C. A. Valentine (2)
Y-12 Central Files

Oak Ridge National Laboratory

R. McClung
D. J. McGuire